



This is a repository copy of *Assessment of energy saving potential of an industrial ethylene cracking furnace using advanced exergy analysis*.

White Rose Research Online URL for this paper:
<http://eprints.whiterose.ac.uk/151053/>

Version: Accepted Version

Article:

Yuan, B., Zhang, Y., Du, W. et al. (2 more authors) (2019) Assessment of energy saving potential of an industrial ethylene cracking furnace using advanced exergy analysis. *Applied Energy*, 254. ISSN 0306-2619

<https://doi.org/10.1016/j.apenergy.2019.113583>

Reuse

This article is distributed under the terms of the Creative Commons Attribution-NonCommercial-NoDerivs (CC BY-NC-ND) licence. This licence only allows you to download this work and share it with others as long as you credit the authors, but you can't change the article in any way or use it commercially. More information and the full terms of the licence here: <https://creativecommons.org/licenses/>

Takedown

If you consider content in White Rose Research Online to be in breach of UK law, please notify us by emailing eprints@whiterose.ac.uk including the URL of the record and the reason for the withdrawal request.



eprints@whiterose.ac.uk
<https://eprints.whiterose.ac.uk/>

Assessment of energy saving potential of an industrial ethylene cracking furnace using advanced exergy analysis

Benfeng Yuan^a, Yu Zhang^a, Wenli Du^a, Meihong Wang^{a, b, *}, Feng Qian^{a, *}

^aState Key Laboratory of Chemical Engineering, East China University of Science and Technology, 130 Meilong Road, Shanghai 200237, China.

^bDepartment of Chemical and Biological Engineering, The University of Sheffield, Sheffield S1 3JD, United Kingdom

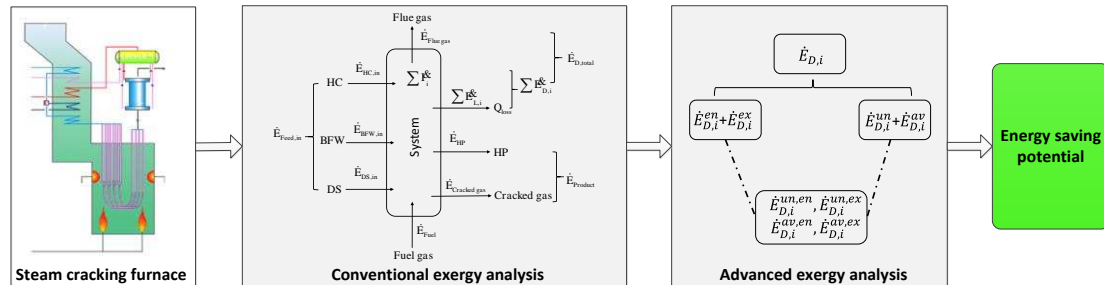
Abstract

Steam cracking furnace is a high energy-consuming equipment in the ethylene plant. Reducing the exergy destruction and losses associated with the steam cracking furnace can increase the thermodynamic efficiency of the system and thereby reducing energy penalties. This paper aims to quantitatively evaluate thermodynamic performance of an industrial steam cracking furnace through conventional and advanced exergy analysis in order to assess its energy saving potential. A steady state simulation of an industrial steam cracking furnace with a total feed capacity of 12t/h was carried out. The simulation was validated by comparing the model prediction results with the industrial data. The conventional exergy analysis shows that the overall exergy efficiency of the steam cracking furnace is found to be 43.43% and the combustion process in the radiation section exhibits the largest exergy destruction followed by the tube reactors in the radiation section. The advanced exergy analysis shows that the combustion process has the highest unavoidable exergy destruction. Moreover, the tube reactors in the radiation section has the highest avoidable exergy

destruction, followed by the combustion process and the feed-steam mixture superheater in the convection section. Therefore, there is high energy saving potential in the tube reactors, combustion process and feed-steam mixture superheater. The advanced exergy analysis also indicates that efforts on improving the radiation and convection sections should be dedicated to themselves while the thermodynamic performance of the quench system should be improved by reducing the exergy destruction of other interacting components.

Keywords: steady state modelling/simulation; thermodynamic performance; conventional exergy analysis; advanced exergy analysis; steam cracking furnace; ethylene manufacturing.

Graphical abstract:



Highlights

- Steady state simulation of steam cracking furnace and model validation
- Simulation considering interactions among Convection and Radiation sections, and Quench system
- Conventional and advanced exergy analysis of a steam cracking furnace
- Combustion process in radiation section exhibits highest exergy destruction followed by tube reactors

- Tube reactors, combustion process and feed-steam mixture superheater have high energy saving potential

1. Introduction

1.1. Background

Nowadays, energy saving has become an important theme. Energy is a commodity that the modern world cannot survive without. However, energy consumption is expected to increase to meet the demand of the population growth in the world. The petrochemical industry is a typical process industry and the total energy consumption accounts for about 20% of total industrial energy consumption in china [1]. Steam cracking is a large energy-consuming process in the petrochemical industries, where the basic chemicals such as ethylene, propylene and some other light olefins are produced. As the heart of this process, steam cracking furnace consumes approximately 65% of the total process energy [2]. Thus, reducing the energy losses associated with the steam cracking furnace is a way to improve the system efficiency.

1.2. Review of model development of steam cracking furnace

Many studies have been performed to model the steam cracking furnace, most of them only focused on the modelling of different components in the steam cracking furnace such as convection section and radiation section.

The initial study on the convection section focused on the macroscopic phenomenon. Liu et al. [3] and Zhou and Yang [4] calculated the heat transfer inside

the tubes of the convection section using Aspen Plus® [5], respectively. Al-Haj Ibrahim et al. [6] carried out a simulation of the whole convection section using a one-dimensional model. With the development of computational fluid dynamics (CFD), more and more attention has been paid to the complicated heat transfer and flow problems in the convection section. De Schepper et al. [7] conducted a CFD study on the gas/vapor-liquid flow regimes during the evaporation process in the convection section. Based on this work, a coupled simulation of the flue gas and process gas in the convection section was performed [8]. Hu et al. [9] carried out a coupled simulation of the convection section, they focused on the temperature profile of the flue gas and the heat flux profile of the external tube wall in the convection chamber.

For study of the radiation section, many achievements have been made in the last two decades. Heynderickx et al. [10], Oprins et al. [11, 12], Stefanidis et al. [13] carried out numerical simulations of the radiation section to study the temperature and flow fields of the flue gas in the furnace, the different combustion mechanisms were also investigated. Lan et al. [14] and Han et al. [15] simulated different types of the cracking furnace using CFD method. Habibi et al. [16] and Hu et al. [17] performed a coupled simulation of the radiation section to study the impact of different radiation models. Zhang et al. [18] proposed an incident radiative heat flux (IRHF) based method to calculate the heat flux profile in the furnace side. The prediction results show that the method overcomes the high computational cost of CFD iterations and has a good accuracy.

1.3. Review of thermal analysis of steam cracking furnace

For confidentiality reasons, only a few articles in the open literature have presented quantitative energy analysis of the steam cracking furnace [2]. Today, the thermal efficiency can be raised above 93% due to the comprehensive use of energy of the steam cracking furnace, most energy saving technologies concentrated on the operation condition optimization and cracking technology. Tuomaala et al. [19] carried out a simulation of the cracking furnace to investigate the impact of the feed rate at range of 25t/h to 28 t/h on the energy efficiency, the results show increasing a hydrocarbon feed rate would result in improved efficiency. In terms of cracking technology, the use of catalysts is known for saving energy, the catalyst can reduce coke formation, which lowers energy efficiency by hindering heat transfer [2].

The energy efficiency assessment and analysis in the previous studies only considers the amount of energy (first law of thermodynamic) but not energy grade (second law of thermodynamics). Exergy analysis can overcome this shortcoming and assess the energy quantitatively and qualitatively [20]. Exergy analysis of the fired heaters has been investigated by several researchers in recent years. Alghany et al. [21] focused on the exergy analysis of the combustion process in the fired heater. Shekarchian et al. [22] performed an exergy analysis of the standalone fired heater to investigate the effect of the heat recovery and preheating techniques on the associated penalties and performance efficiency, the results show the heat recovery and preheating techniques can improve the system performance dramatically. Unlike the common fired heater, steam cracking furnace is a special fired heater with a complex heat exchange

system and the cracking process. Alizadeh et al. [23] made conventional exergy analysis of both the radiation section and the convection section in the steam cracking furnace to study the effect of varying operation conditions on the exergy efficiency of the whole furnace.

However, conventional exergy analysis only determines the thermal inefficiency of the system while it cannot identify the share of inefficiencies that can be avoided and analyse the interactions between the components of the system [24]. Advanced exergy analysis is used to address this issue, which further determines how much of the exergy destruction identified by the conventional exergy analysis is avoidable and how much is caused by the structure or operation conditions of the component itself. This approach splits the exergy destruction of the system components into endogenous/exogenous and avoidable/unavoidable parts [24, 25]. Advanced exergy analysis has been applied to many industrial systems such as natural gas liquefaction[26], refrigeration system[27, 28], power plant[29] and so on.

1.4. Motivation, aim and novel contributions of this study

As reported in literatures [2, 30], the energy efficiency of the steam cracking furnace can reach above 93% while the exergy efficiency is below 50%. In terms of the energy efficiency, the steam cracking furnace has a high performance. Energy analysis based on First Law of Thermodynamics can no longer give any substantial suggestions for improvement. However, in terms of the exergy efficiency, exergy analysis can provide more significant guidance in the improvement of the steam cracking furnace.

In addition, from the previous studies reviewed in Section 1.3, there is no publication on the conventional exergy analysis of all the three sections of the steam cracking furnace considering their internal interactions. There is also no publication on the advanced exergy analysis applied to any sections or the whole of the steam cracking furnace so far.

To fill these gaps, this paper aims to perform conventional and advanced exergy analysis of the whole steam cracking furnace in order to quantify its energy saving potential. The novel contributions of this research are listed as follow:

- (1) A steady state model for the whole steam cracking furnace was developed, which considered interactions among three different sections;
- (2) Conventional exergy analysis for the steam cracking furnace was carried out, the thermodynamic inefficiency for each component were analysed;
- (3) Based on convectional exergy analysis, advanced exergy analysis was performed to further determine the energy saving potential of each component.

2. Model development and model validation

2.1. Process description of steam cracking furnace

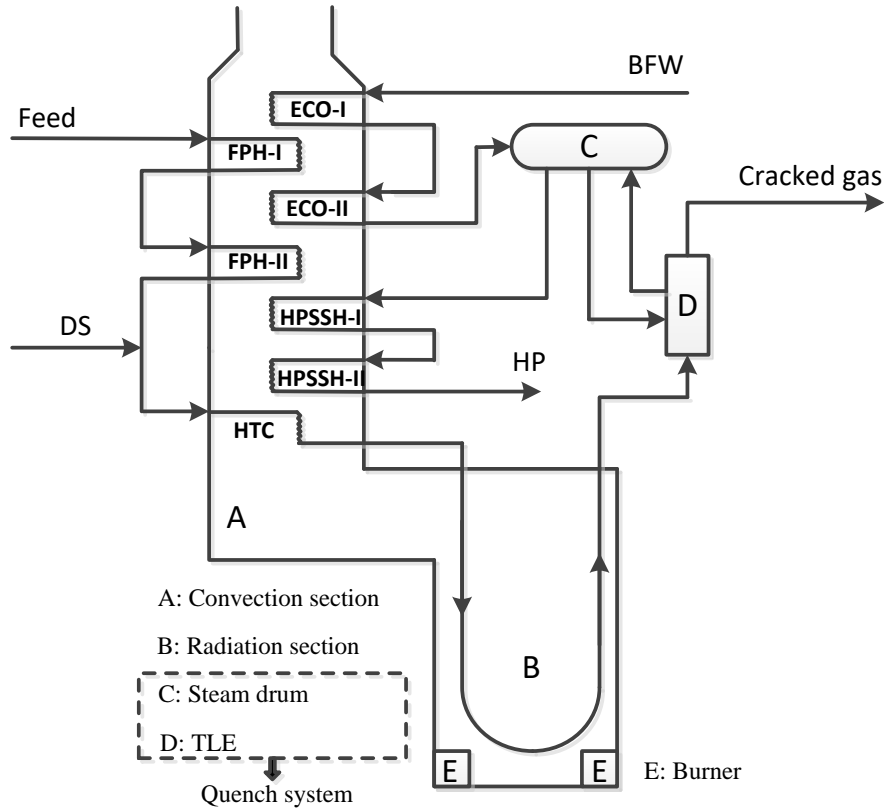


Fig. 1. Flow diagram of an industrial steam cracking furnace

A steam cracking furnace with the feedstock of ethane and propane, as shown in Fig. 1, consists of three sections: convection section, radiation section and quench system [31]. The convection section contains several sub-sections: the economizer (ECO-I, II), feed preheater (FPH-I, II), high pressure steam superheater (HPSSH-I, II) and feed-steam mixture superheater (HTC) [9, 31]. The radiation section contains the tubular reactors (furnace and coils) and the burner. The fuel combustion in the burner supplies the heat for the cracking process in the tube reactors. The remaining heat in the high-temperature flue gas stream goes into the convection section. In the convection

section, the hydrocarbon feedstock (HC) is preheated in FPH sub-section. After mixing with the dilute steam (DS), the process gas (HC+DS) enters HTC sub-section for further heating and finally leaves the convection section at around 570-670°C. The quench system contains two components: steam drum and transfer line exchanger (TLE). The cracked gases leave the radiation coil at around 750-875 °C . To preserve their composition, the cracked-gas temperature must be cooled rapidly by exchanging heat with the saturated water at around 9-12MPa from the steam drum. The generated high-pressure steam (HP) enters HPSSH sub-section for further heating to 520°C and then is merged into the steam pipe network.

2.2. Model development of steam cracking furnace

Steady state first principle models for all the three sections were developed based on thermal coupling of the tube and the furnace/convection chamber. Thus, the tube and the furnace/convection chamber were modelled respectively, as shown in Fig. 2

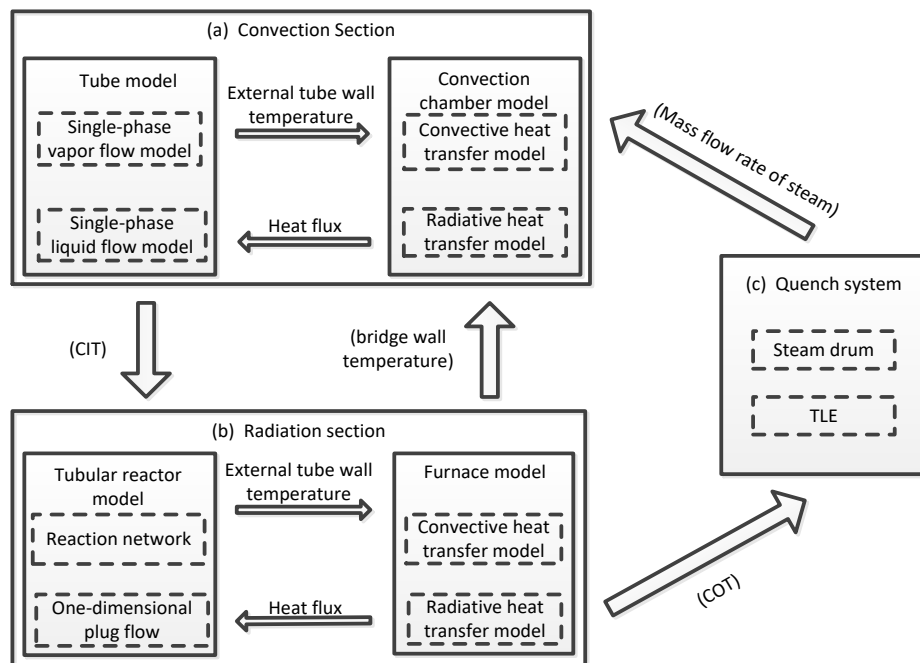


Fig. 2. Model structure of the steam cracking furnace (a) model for the convection section, (b) model for the radiation section, (c) model for the quench system

2.2.1. Convection section

As shown in Fig. 2(a), the convection section was simulated by thermal coupling of the tube and convection chamber. Therefore, the tube and convection chamber were modelled respectively in this work.

2.2.1.1. Development of the tube model

Due to a large length to inner diameter ratio of the tube, the fluid flow inside the tube can be assumed as ideal plug flow. In addition, there is no reaction in the convection section. Consequently, the change in component concentration along the tube axial and radial directions can be ignored. The steady-state conservations for the momentum and energy are given by Eqs. (1) and (2):

$$\frac{dp}{dz} = - \left(\frac{2f}{d} + \frac{\xi}{\pi r_b} \right) \rho u^2 - \rho u \frac{du}{dz} \quad (1)$$

$$\sum_i F_i c_{pi} \frac{dT}{dz} = \pi dq \quad (2)$$

where d is the inner diameter of the tube, r_b is the radius of the bend, q represents the total heat flux on the internal surface of the tube, which is calculated from the total heat flux q_{flux} (on the external surface of the tube) via the convection chamber simulation, by the following expression $\frac{q}{q_{flux}} = \frac{D}{d}$. Based on the fluid temperature inside the tube, the tube metal temperature T_w needed for the convection chamber simulation can be calculated by Eq. (3):

$$q = (T_w - T) \left(\frac{1}{h_c} + \frac{d}{2\lambda_w} \ln \frac{D}{d} \right)^{-1} \quad (3)$$

where h_c is the convective heat transfer coefficient inside the tube, which is calculated by Dittus-Boelter correlation [32]. Therefore, with a certain q_i provided by the convection chamber simulation, an updated tube metal temperature profile can be obtained from the tube simulation using Eqs. (1)-(3), which in turn affects the convection chamber simulation.

2.2.1.2. Development of convection chamber model

The convection chamber model is used to calculate the heat flux on the external surface of the tube used for the tube simulation. A heat transfer analysis (HTA) model was developed for the heat transfer calculation in the tube bundle. Through the analysis of the heat transfer process in the convection section, the heat flux on the external surface of the tube can be given by Eq. (4):

$$q_{\text{flux}} = \frac{Q_{\text{flue}}^{\text{con}} + Q_{\text{flue}}^{\text{rad}} + Q_{\text{wall}}^{\text{rad}}}{A} \quad (4)$$

where $Q_{\text{flue}}^{\text{con}}$ and $Q_{\text{flue}}^{\text{rad}}$ represent the convective heat and the radiative heat transferred to the external tube wall from the flue gas, respectively. $Q_{\text{wall}}^{\text{rad}}$ is the radiative heat transferred to the external tube wall from the furnace wall.

The convective heat transferred to the tube from the flue gas can be written as:

$$Q_{\text{flue gas}}^{\text{con}} = h_f A (T_g - T_w) \quad (5)$$

where h_f is the convective heat transfer coefficient of the flue gas through the tube bundle. Many experimental and numerical studies have been conducted to investigate the convective heat transfer of the gas through the tube bundle [33, 34]. A correlation

[35] suitable for the tube bundles with the in-line and staggered arrangements was adopted to calculate the convective heat transfer coefficient in the convection chamber, given by Eq.(6).

$$h_c = 0.33C_H\psi\frac{\lambda}{d}(\text{Re})^{0.6}(\text{Pr})^{0.8} \quad (6)$$

where the parameters, C_H and ψ , are related to the tube arrangement, ratio of tube pitch to tube diameter.

Due to the numerous tubes in the tube bundle, the contact area of the flue gas and the tube wall is very large. Thus, the radiation view factor can be considered to equal one and the radiation form between the flue gas and the tube wall is considered as the radiation between the gas and the shell. The radiative heat transfer equation of the flue gas is determine as the following based on Hottel's model [32].

$$Q_{\text{flue gas}}^{\text{rad}} = \sigma\left(\frac{1+\varepsilon_t}{2}\right)A(\varepsilon_g T_g^4 - \alpha_g T_w^4) \quad (7)$$

The radiative heat transfer from the furnace wall to the tube can be taken as the radiative heat transfer between two parallel planes (a virtually hot plane and a virtually cold plane). Eq. (7) gives the radiative heat transfer equation between infinite parallel planes:

$$Q_{\text{wall}}^{\text{rad}} = \sigma AN(T_{\text{wall}}^4 - T_w^4) \quad (8)$$

where N is the total exchange factor, which is given by the following equation [36].

$$N = 1/((1-\varepsilon_w)/\varepsilon_w + 1/F + (1-\varepsilon_t)/\varepsilon_t) \quad (9)$$

2.2.2. Radiation section

The radiation section was also simulated by thermal coupling of the tube reactor

and furnace.

2.2.2.1. Development of tube reactor model

In the tube reactor side, as the tube reactors with large length to inner diameter ratio, the process gas flow inside the reactor coils can be assumed as ideal plug flow [18]. To simplify the calculation, this assumption was adopted in the present study, as shown in Fig. 2(b). The tube reactor was modeled using the commercial software package Coilsim1D [37, 38]. The software Coilsim1D was developed by Ghent University in Belgium and was specially used for simulation of the tube cracking reactor. It has an extensive reaction network comprising hundreds of species and thousands of elementary reactions. Similar to the tube model in the convection, the tube metal temperature T_w needed for the furnace model is calculated by the tube reactor model in the radiation section. The modeling process using the software Coilsim1D has been discussed in literature[18].

2.2.2.2. Development of furnace model

The steady-state energy balance in the furnace can be written as:

$$Q_r = Q_{ab} + Q_{loss} + Q_{flue} \quad (10)$$

where Q_r is the total heat release from the fuel combustion, Q_{ab} represents the heat absorbed by all reactor coils, Q_{flue} is the enthalpy change between the inlet fuel and air entering the furnace and the hot flue gas leaving the furnace and Q_{loss} is the heat loss through the furnace refractory.

An incident radiative heat flux (IRHF) based method proposed by Zhang et al. [18] was adopted to calculate the heat flux profile in the furnace side. In IRHF method, a

novel correlation between the heat flux profile on the external surface of the tube and IRHF was developed by an overall zero-dimensional heat balance. The heat balance equation can be written as:

$$q_{\text{flux}} = (\varepsilon_w q_{\text{inci}} - \varepsilon_w \sigma T_w^4)(1 + \beta) \quad (11)$$

where β is a constant factor relating the convective heat flux to the net radiative heat flux. q_{inci} is the incident radiative heat flux of the flue gas, which can be updated by the following expression $q_{\text{inci,new}} = \alpha q_{\text{inci,orig}}$. α is a scaling factor defined as:

$$\alpha = \left(1 + \frac{\Delta T_{\text{flue}}}{T_{\text{flue,ori}}} \right) \quad (12)$$

where ΔT_{flue} is the difference between the flue gas bridge wall temperature (flue gas temperature leaving the radiation section) at the new and the original operating conditions ($T_{\text{flue,new}}$ and $T_{\text{flue,ori}}$).

The original IRHF, heat flux and flue gas bridge wall temperature were calculated by CFD method as a base case. With a certain T_w , an initial flue gas bridge wall temperature T_{flue} can be obtained using Eq. (9). Through Eqs. (10)-(11), a new heat flux profile of the external surface of the tube can be calculated. Therefore, a new flue gas bridge wall temperature can be obtained using Eq. (9) again. The iteration continues until the difference of the flue gas bridge wall temperatures between two iterations is within 1K. Finally, an updated heat flux profile on the external surface of the tube can be obtained, which in turn affects the tube simulation.

2.2.3. Quench system

Quench system includes steam drum and TLE. The water in the steam drum is the

saturate water at 324°C. The saturate water flows into TLE, exchanging heat with the cracked gas. The generated steam flows back to the steam drum and then enters HPSSH section for further heating. Thus in TLE, a vapor liquid two-phase flow occurs in the water side. Some correlations describing the convective heat transfer coefficient in the boiling process can be found in literatures [39, 40]. In the cracked gas side, the reactor model in the radiation section can be used here to calculate the temperature profile and the heat flux profile. The simulation of TLE was also carried out using the commercial software package Coilsim1D developed by Ghent University in Belgium.

2.3. Operating conditions and solution strategy for simulation

2.3.1. Operating conditions

All the relevant information about the steam cracking furnace in this work was provided by a petrochemical company. Due to the corporate intellectual property and technical know-how, only the geometry dimension and industrial data of the cracking furnace can be provided.

To carry out the steady state simulation of the convection section, the inlet conditions of HC, DS, boiler feed water (BFW) and the flue gas should be taken as input data. The inlet conditions of HC and DS are shown in Table 1 and the compositions of HC is shown in Table 2. The inlet temperature and mass flow rate of the flue gas leaving the radiation section are calculated through the steady state model of the radiation section. To carry out the steady state simulation of the radiation section, the inlet conditions of the process gas and the fuel gas should be taken as the input data.

The information of the fuel gas is shown in Table 1, the inlet conditions of the process gas are calculated through the steady state model of the convection section. The input data of the quench system is from the steady state simulations of the convection and radiation sections. The detailed geometry parameters of the whole furnace (including convection section, radiation section and TLE) are shown in Tables 1S-3S in the supplementary material.

2.3.2. Simulation solution strategy

Iterations are necessary in the simulation process. For simulation of the convection and the radiation sections, the external tube skin temperature profile is initialized. Through the convection chamber/furnace model, the heat flux profile of the external tube wall is calculated and given to the tube model. Then a new external tube skin temperature profile can be calculated using the tube model. The iteration is repeated until the difference of each external tube skin temperature between two iterations is less than 1K.

Iterations are also necessary to simulate the whole furnace. The calculation steps are listed as follow:

- (1) Initializing the coil inlet temperature (CIT) of the process gas in the radiation section
- (2) Carrying the simulations of the radiation section and quench system, outputting the bridge wall temperature, the mass flow rate of the flue gas and the amount of the generated steam.

- (3) Carrying out the simulation of the convection section, getting a new CIT
- (4) Repeating steps (2)-(3) until the difference of CIT between two iterations is less than 1K.

Table 1. Inlet conditions for simulation of the steam cracking furnace

| Description | Value |
|--|--------|
| HC mass flow rate (kg/h) | 12,800 |
| HC inlet temperature in FPH section (°C) | 80 |
| HC inlet pressure in FPH section (MPa) | 0.83 |
| DS mass flow rate (kg/h) | 4,480 |
| DS inlet temperature (°C) | 185 |
| DS inlet pressure (MPa) | 0.385 |
| BFW inlet temperature (°C) | 91.5 |
| BFW inlet pressure (MPa) | 9.9 |
| COT (°C) | 847.20 |

Table 2. Compositions of the hydrocarbon feedstock and the fuel gas

| Hydrocarbon feedstock | | | |
|-------------------------------|-------------------------|--------------------------------|-------------------------|
| Component | Mass fraction (wt/wt) | Component | Mass fraction (wt/wt) |
| C ₂ H ₆ | 0.8 | C ₃ H ₈ | 0.2 |
| Fuel gas | | | |
| Component | Mole fraction (mol/mol) | Component | Mole fraction (mol/mol) |
| H ₂ | 0.0985 | C ₃ H ₈ | 0.0011 |
| CO | 0.0016 | C ₃ H ₆ | 0.0032 |
| CH ₄ | 0.8930 | C ₂ H ₂ | 0.0003 |
| C ₂ H ₆ | 0.0017 | C ₄ H ₁₀ | 0.0001 |
| C ₂ H ₄ | 0.0005 | | |

2.4. Model validation

Table 3 shows some process data collected from the industrial ethylene plant. As shown in Table 3, the validation is performed by comparing the model prediction results with the industrial data. As not every stream has the measurement point in the industrial site, only some of industrial data is given to compare with the model prediction results. As mentioned above, the mass flow rates of BFW/HP and the fuel gas depend on the exchanged heat in TLE and COT, respectively. The prediction results of the mass flow

rates of BFW/HP and the fuel gas are close to the data from the industry. Table 3 also shows the temperature distributions of the process gas side and the flue gas side. For the process gas side, the maximum relative error of the outlet temperature is 4.08% and the others are within 4%. For the flue gas side, the maximum relative error of the outlet temperature is 8.4% and the others are within 4.5%. The product yields predicted by the steady state simulation are also in good agreement with the industrial data. Especially for the key product such as ethylene, the relative error is less than 1.5%. The validation proves that the data set produced by the steady state model of the whole steam cracking furnace are reliable.

Table 3. Comparison between the modeling results and industrial data

| Mass flow rate (kg/h) | | | |
|--|-----------------|-------------------|--------------------|
| Streams | Industrial data | Predicted results | Relative error (%) |
| BFW | 12,171 | 12,717.00 | -4.49 |
| HPSSH | 13,393 | 13,062.20 | -2.47 |
| Fuel gas | 1,628.40 | 1,848 | 13.79 |
| Outlet temperature of process gas in each component (°C) | | | |
| Main components | Industrial data | Predicted results | Relative error (%) |
| ECO2 | 256.7 | 266.84 | 3.95 |
| FPH2 | 459.6 | 440.85 | -4.08 |
| HPSSH1 | 403.1 | 412.24 | 2.27 |
| HPSSH2 | 498.1 | 498.08 | 0.00 |
| HTC1 | 637.7 | 650.28 | 1.97 |
| TLE | 508 | 500.3 | -1.52 |
| Outlet temperature of flue gas in each component (°C) | | | |
| Main components | Industrial data | Predicted results | Relative error (%) |
| ECO1 | 127.30 | 122.12 | -4.07 |
| FPH1 | 184.95 | 189.64 | 2.54 |
| ECO2 | 245.35 | 255.74 | 4.23 |
| FPH2 | 378.5 | 410.31 | 8.40 |
| HPSSH1 | 606.08 | 612.66 | 1.09 |
| HPSSH2 | 790.00 | 793.97 | 0.50 |
| HTC1 | 1,037 | 1,062.10 | 2.42 |
| Out pressure of Process gas (Mpa) | | | |
| Main components | Industrial data | Predicted results | Relative error (%) |
| HPSSH2 | 9.78 | 9.84 | 0.06 |

| HTC | 2.62 | 2.71 | 3.44 |
|-----------------------------------|---------------------------|-------------------|--------------------|
| Main components | Production yield (wt/wt%) | | |
| | Industrial data | Predicted results | Relative error (%) |
| H ₂ | 3.12 | 3.40 | 8.97 |
| CH ₄ | 9.8 | 10.19 | 4.02 |
| C ₂ H ₄ | 49.98 | 49.37 | -1.22 |
| C ₂ H ₆ | 30.71 | 27.06 | -11.90 |
| C ₃ H ₆ | 2.31 | 2.12 | -8.23 |
| C ₃ H ₈ | 0.82 | 0.72 | -12.80 |
| 1,3-C ₄ H ₆ | 1.29 | 1.61 | 24.81 |
| 1C ₄ H ₈ | 0.28 | 0.24 | -1.25 |

3. Methodology

In this section, the conventional and advanced exergy analysis is used to calculate the exergy destruction and assess the energy saving potential of the steam cracking furnace.

3.1. Conventional exergy analysis

Exergy is defined as the maximum work which is obtained when the system is brought to a state of thermodynamic equilibrium with the common components of the natural surroundings by means of reversible processes[41]. For a steady-state system, exergy of process streams mainly includes physical exergy (\dot{E}^{TP}) and chemical exergy (\dot{E}^{ch}).

Physical exergy is defined that the work is obtained by taking the system from the process state (T, P) to the reference environment state (T_0, P_0) [42]. The physical exergy is expressed by the following equation.

$$\dot{E}^{FP} = H(T, P, z) - H(T_0, P_0, z) - T_0 (S(T, P, z) - S(T_0, P_0, z)) \quad (13)$$

where H and S are the enthalpy and entropy of the system, respectively. In this work, the natural environment (25°C, 1atm) of the steam cracking furnace is chosen as the

reference environment state.

Chemical exergy is the work that can be obtained by taking a substance from the environmental state to the standard dead state [42]. The chemical exergy is given in Eq. (14).

$$E^{ch} = \sum_{i=1}^n y_i (X_i^0 + RT \ln y_i) \quad (14)$$

In this equation, the first item on the right side represents the exergy change caused by chemical reaction, the second item represents the exergy change caused by the concentration change. X_i^0 is the molar standard chemical exergy, which is defined as follows:

$$X_i^0 = \Delta G_f^0 + \sum_{j=1}^{n,i} n_{i,j} X_j^0 \quad (15)$$

To calculate the chemical exergy, the standard substances in the environment should be determined. The chemical exergy of reference for substances reported by Szargut et al.[41] is adopted. In the steam cracking furnace, the chemical reaction occurs in two process: combustion of the fuel gas and cracking reaction of the hydrocarbon feedstock. Table 2 gives the detailed components of the fuel gas. To calculate the chemical exergy of the products, the chemical composition of the cracked gas should also be determined. The cracked gas contains about eighty components, among which the mass fraction of the common fifteen components exceed 98.5%. Thus, these fifteen components are selected to represent the final products, as shown in Table 4.

Table 4. The selected components for representing the cracked gas

| Number | Component | Number | Component |
|--------|--|--------|---|
| 1 | Hydrocarbon (H ₂) | 9 | Butadiene (1,3-C ₄ H ₆) |
| 2 | Methane (CH ₄) | 10 | Butene (1-C ₄ H ₈) |
| 3 | Acetylene (C ₂ H ₂) | 11 | Butane (n-C ₄ H ₁₀) |
| 4 | Ethylene (C ₂ H ₄) | 12 | Isoprene (C ₅ H ₈) |
| 5 | Ethane (C ₂ H ₆) | 13 | Cyclopentadiene(C ₅ H ₈) |
| 6 | Propylene (C ₃ H ₆) | 14 | Benzene (C ₆ H ₆) |
| 7 | Propane (C ₃ H ₈) | 15 | Toluene (C ₇ H ₈) |
| 8 | Styrene (C ₈ H ₈) | | |

The rational exergy efficiency [43] was adopted in this study. The rational exergy efficiency is the ratio of the exergy desired output to the used exergy, the expression is given by:

$$\varepsilon_{\text{rat}} = \frac{\text{Desired output exergy}}{\text{Used exergy}} = \frac{\dot{E}_{\text{Desired output}}}{\dot{E}_{\text{Used}}} \quad (16)$$

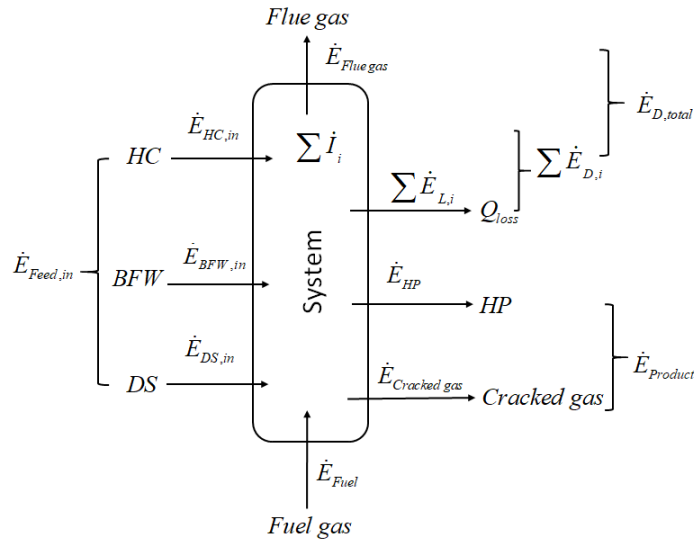


Fig. 3. A general presentation of exergy flow process in the steam cracking furnace

Fig. 3 shows the exergy flow processes for the whole steam cracking furnace. Similar as the energy balance, an exergy balance for the whole furnace can be built as shown in Eq. (17).

$$\dot{\mathcal{E}}_{\text{Feed,in}} + \dot{\mathcal{E}}_{\text{Fuel}} = \dot{\mathcal{E}}_{\text{Product}} + \dot{\mathcal{E}}_{\text{D,total}} \quad (17)$$

According to Eq. (16), the desired output exergy and the used exergy for the whole steam cracking furnace are expressed as:

$$\dot{\mathcal{E}}_{\text{Desired output}} = \dot{\mathcal{E}}_{\text{Product}} - \dot{\mathcal{E}}_{\text{Feed,in}} \quad (18)$$

$$\dot{\mathcal{E}}_{\text{Used}} = \dot{\mathcal{E}}_{\text{Fuel}} \quad (19)$$

Thus, the rational exergy efficiency for the whole steam cracking furnace is calculated by Eq. (20).

$$\varepsilon_{\text{whole furnace}} = \frac{\dot{\mathcal{E}}_{\text{Product}} - \dot{\mathcal{E}}_{\text{Feed,in}}}{\dot{\mathcal{E}}_{\text{Fuel}}} = \frac{\dot{\mathcal{E}}_{\text{Cracked gas}} + \dot{\mathcal{E}}_{\text{HP}} - \dot{\mathcal{E}}_{\text{HC,in}} - \dot{\mathcal{E}}_{\text{BFW,in}} - \dot{\mathcal{E}}_{\text{DS,in}}}{\dot{\mathcal{E}}_{\text{Fuel}}} \quad (20)$$

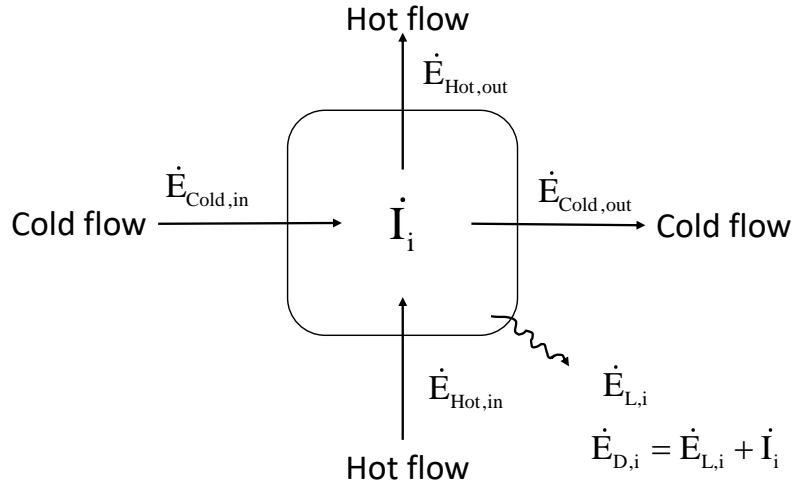


Fig. 4. A general presentation of exergy flow process in single component

All the components in the steam cracking furnace can be taken as a heat exchanger except for the combustion process in the burner. Fig. 4 shows the exergy flow processes of these components, the rational exergy efficiency of the *i*th component can be given as [44] :

$$\varepsilon_i = \frac{\dot{\mathcal{E}}_{\text{Desired out},i}}{\dot{\mathcal{E}}_{\text{Used},i}} = \frac{\dot{\mathcal{E}}_{\text{Cold,out}} - \dot{\mathcal{E}}_{\text{Cold,in}}}{\dot{\mathcal{E}}_{\text{Hot,in}} - \dot{\mathcal{E}}_{\text{Hot,out}}} \quad (21)$$

In order to analyse the distribution of the exergy destruction of the whole furnace, the ratio of the exergy destruction within i th component to the used exergy is also given as

$$y_{D,i} = \dot{E}_{D,i} / \dot{E}_{Used} = \dot{E}_{D,i} / \dot{E}_{Fuel} \quad (22)$$

3.2. Advanced exergy analysis

Through advanced exergy analysis, the exergy destruction within the system components can be split into endogenous/exogenous and avoidable/unavoidable parts, which is explained in detailed in Ref. [44].

Endogenous exergy destruction ($E_{D,i}^{EN}$) is due to the irreversibility's inside the component while the exogenous part of the variable ($E_{D,i}^{EX}$) is imposed on the component by other components [29].

$$\dot{E}_{D,i} = \dot{E}_{D,i}^{EN} + \dot{E}_{D,i}^{EX} \quad (23)$$

The unavoidable exergy destruction ($E_{D,i}^{UN}$) cannot be reduced due to technological limitations, such as availability and costs of materials and manufacturing methods [45].

The avoidable part ($E_{D,i}^{AV}$) is the difference between the total and unavoidable exergy destruction as shown in Eq. (13).

$$\dot{E}_{D,i} = \dot{E}_{D,i}^{UN} + \dot{E}_{D,i}^{AV} \quad (24)$$

3.2.1. Combining the two splitting approach

For better insight of the efficiency assessment of the thermal system, the endogenous and exogenous exergy destruction can also be further divided into the avoidable and unavoidable parts, such as unavoidable endogenous exergy destruction

$(E_{D,i}^{UN,EN})$, avoidable endogenous exergy destruction ($E_{D,i}^{AV,EN}$), unavoidable exogenous exergy destruction ($E_{D,i}^{UN,EX}$) and avoidable exogenous exergy destruction ($E_{D,i}^{AV,EX}$) [24].

The four splitting combinations can be calculated as:

$$\dot{E}_{D,i}^{UN} = \dot{E}_{P,i} \left(\dot{E}_{D,i} / \dot{E}_{P,i} \right)^{UN} \quad (25)$$

$$\dot{E}_{D,i}^{UN,EN} = \dot{E}_{P,i}^{EN} \left(\dot{E}_{D,i} / \dot{E}_{P,i} \right)^{UN} \quad (26)$$

$$\dot{E}_{D,i}^{UN,EX} = \dot{E}_{D,i}^{UN} - \dot{E}_{D,i}^{UN,EN} \quad (27)$$

$$\dot{E}_{D,i}^{AV,EN} = \dot{E}_{D,i}^{EN} - \dot{E}_{D,i}^{UN,EN} \quad (28)$$

$$\dot{E}_{D,i}^{AV,EX} = \dot{E}_{D,i}^{UN,EX} - \dot{E}_{D,i}^{UN,EN} \quad (29)$$

The ratio $(\dot{E}_{D,i}/\dot{E}_{P,i})$, $\dot{E}_{P,i}^{EN}$ and $\dot{E}_{D,i}^{EN}$ are first determined from the unavoidable and theoretical processes.

According to the above equations, the benefit of the advanced exergy analysis is obvious over the conventional exergy analysis. The advanced exergy analysis can provide some improvements for designers and find some places where the improvements are required. For example, $E_{D,i}^{AV,EN}$ determines the amount of exergy destruction due its own irreversibility which can be reduced by improving the component efficiency. $E_{D,i}^{AV,EX}$ determines the amount of exergy destruction which can be reduced by improving other components' efficiency.

3.2.2. Conditions for splitting exergy destruction

In general, for splitting the exergy destruction into endogenous and exogenous parts, the assumption for different components should be made: $\dot{E}_{D,i} = 0$ or $\dot{E}_{D,i} = \min$. For the steam cracking furnace, both the convection section and the quench

system are treated as the heat exchanger. As for single heat exchanger, both pressure drops (Δp) and minimum temperature difference at the pinch point (ΔT_{min}) should equal zero. However, the convection section is composed of several heat exchangers in series and these heat exchangers are rather complicated, because the theoretical condition of a concurrent heat exchanger may affect its surrounding heat exchangers since the temperature of the process gas inside the tube out of the heat exchanger working theoretically may exceed the allowed temperature of its following heat exchanger or the temperature of the flue gas entering its successive heat exchanger may be lower than the corresponding process gas temperature[29]. As shown in Fig. 5, one reversible adiabatic heater (RAH) is added before each heat exchanger and the target of each heater is set to heat the working fluid to a specified temperature[29, 44, 46]. The RAHs are not considered under the real condition. In this way, the heat utilized by the process gas inside the tube is calculated firstly and then the temperature of the flue gas entering the heater can be obtained with the pre-calculated mass flow rate of the flue gas from the heat balance. For the radiation section, the fuel gas combustion and the cracking reaction occur in this section, the conditions ($\dot{E}_{D,i}=0$ or $\varepsilon_i=1$) can be achieved only through fulfilling the exergy balance for the component ($\dot{E}_{F,i} = \dot{E}_{P,i}$), and by ignoring the mass and energy balances. A detailed description is given by literatures[47, 48].

For the unavoidable/avoidable exergy destruction, the best performance characteristics can be derived with investment-efficiency consideration or based on the understanding and practical experience of the designer[29]. For all heat exchangers in the convection section, the minimum approach temperature difference (ΔT_{min}) is set to

be equal to 5 °C. In the radiation section, the flue gas supplies the heat for the cracking process inside the tube. Thus, the radiation section can be considered as one heat exchanger which has a chemical reaction inside the tube and the unavoidable condition can be define: $\Delta T_{min} = 10\text{ }^{\circ}\text{C}$. Exergy destruction in the combustion process is mainly affected by the excess air fraction and the inlet temperature of the air. The thermodynamic inefficiencies of combustion can be reduced by preheating the combustion air and reducing the oxygen excess ratio. Thus, the air inlet temperature of 200 °C and oxygen excess ratio of 1.1 are selected as the unavoidable condition of the combustion process.

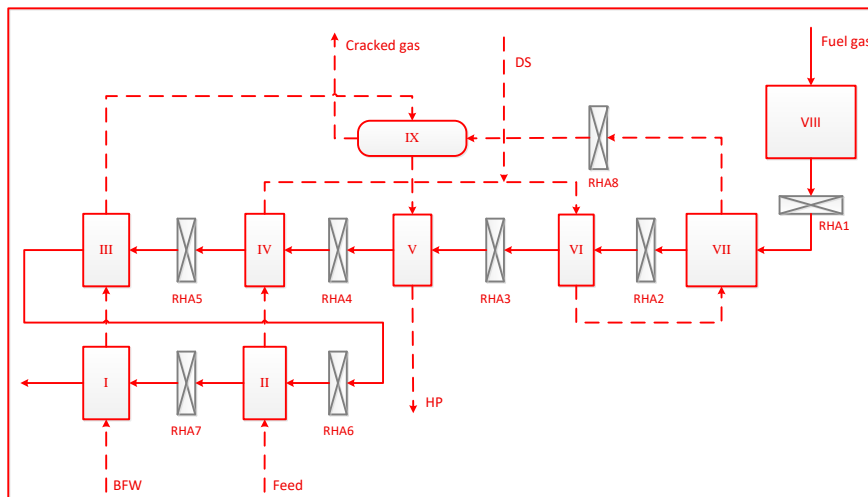


Fig. 5. Simplified flow diagram of a steam cracking furnace for advanced exergy analysis (I-ECO-I, II-FPH-I, III-ECO-II, IV-FPH-II, V-(HPSSH-I, II), VI-HTC, VII-tube reactors, VIII-burner, IX-quench system)

4. Results and discussion

4.1. Conventional exergy analysis

The results of conventional exergy analysis at the component level are presented in Table 5. The rational exergy efficiency of the steam cracking furnace is about 43.43% which means there is a large space to improve the thermodynamic performance of the steam cracking furnace. Table 5 shows the total exergy destruction within the convection section is 2,309.46 kW, larger than that within the quench system (746.97 kW) but much lower than that within the radiation section (11677.38 kW). In addition, the exergy destruction caused by the heat loss is 921.56 kW. It can be found by the exergy destruction ratio ($y_{D,i}$), the total exergy destruction within the convection section accounts for 8.31% of the fuel exergy while the exergy destructions within the radiation section and the quench system account for 41.98% and 2.69%, respectively.

4.1.1. Convection section

As shown in Table 5, Sub-sections I and III have high exergy efficiencies (81.38%, 82.66%). This is because Sub-sections I and III, where the heat transfer is due to single phase liquid forced convection, has a larger heat transfer efficiency than the other sub-sections where the heat transfer is due to single phase vapor forced convection. Moreover, Sub-sections I, III and V (81.38%, 82.66% and 76.06%), where the water or steam stream flows through, has a higher exergy efficiency than Sub-sections II, IV and VI (41.65%, 67.45% and 67.73%) where the hydrocarbon gas feedstock flows through. This is because both the water and steam have a larger heat capacity than the gas

mixture of the ethane and propane, improving the heat transfer efficiency. Table 5 also shows the exergy destruction of the sub-sections where the same stream flows through, such as Sub-sections II (190.19 kW), IV (532.24 kW) and VI (943.46kW), increases from top to bottom. The same goes for Sub-sections I (46.54 kW), III (177.51 kW) and V (419.51 kW), where the water/steam stream flows through. This can be explained by literature [44], a larger temperature difference leads to a larger exergy destruction in the heat exchangers. As shown in Fig. 6, the temperature differences of the sub-sections gradually increase from top to bottom in the convection section.

4.1.2. Radiation section

Table 5 also shows the thermodynamic inefficiencies of Sub-sections VII and VIII in the radiation section. The exergy destruction (3,057.55 kW) within Sub-section VII (i.e. tube reactors), in which the radiative heat transfer is prevailing, is obviously larger than those in the convection section where the convective heat transfer is prevailing. The reason for this can be clearly explained by Fig. 6 that the radiative heat transfer can be the main heat transfer type only when the temperature of the flue gas is extremely high, causing the large temperature difference between the flue gas and the process gas. Additionally, the heat released from the hot side to the cold side by form of radiation is far much intensive than that by form of the convection, which also increases the exergy destruction.

In Sub-section VIII (i.e. burner), the combustion process contributes the largest exergy destruction (8,619.83 kW), accounting for 55.06% of the total exergy

destruction (15,655.41 kW) of the whole furnace. It can also be found by the exergy destruction ratio ($y_{D,i}$), about 31.15% of the fuel exergy is consumed in the combustion process.

4.1.3. Quench system

As shown in Table 5, the exergy efficiency (79.10%) of the quench system is obviously higher than those of most sub-sections. This is because in the quench system, the saturate water is used to cool the cracked gas rapidly from 850°C to 500°C. The evaporation of the saturate water promotes the heat transfer efficiency of the water side, leading to a high exergy efficiency.

Table 5. Results of conventional exergy analysis of the steam cracking furnace

| Comp | $\dot{E}_{F,i}$ (kW) | $\dot{E}_{P,i}$ (kW) | $\dot{E}_{D,i}$ (kW) | ε_i (%) | y_i (%) |
|--------------------|--------------------------------|----------------------|----------------------|---------------------|-----------|
| Convection section | | | | | |
| I | 249.95 | 203.41 | 46.54 | 81.38 | 0.17 |
| II | 325.95 | 135.77 | 190.19 | 41.65 | 0.69 |
| III | 1,023.68 | 846.17 | 177.51 | 82.66 | 0.64 |
| IV | 1,635.32 | 1,103.07 | 532.24 | 67.45 | 1.92 |
| V | 1,752.16 | 1,332.65 | 419.51 | 76.06 | 1.52 |
| VI | 2,924.03 | 1,980.57 | 943.46 | 67.73 | 3.41 |
| Radiation section | | | | | |
| VII | 10,973.62 | 7,916.07 | 3,057.55 | 72.14 | 11.05 |
| VIII | 27,817.00 | 19,197.17 | 8,619.83 | 69.01 | 31.15 |
| Quench system | | | | | |
| IX | 3,518.75 | 2,826.85 | 746.97 | 79.10 | 2.70 |
| streams | Input exergy (kW) | | streams | Output exergy(kW) | |
| HC | 176164.23 | | HP | 5171.09 | |
| DS | 904.97 | | Cracked gas | 184062.03 | |
| BFW | 143.79 | | Flue gas | 352.73 | |
| Fuel gas | 27675.58 | | Q_{loss} | 568.83 | |
| The whole furnace | Rational exergy efficiency (%) | | | | |
| | 43.43 | | | | |

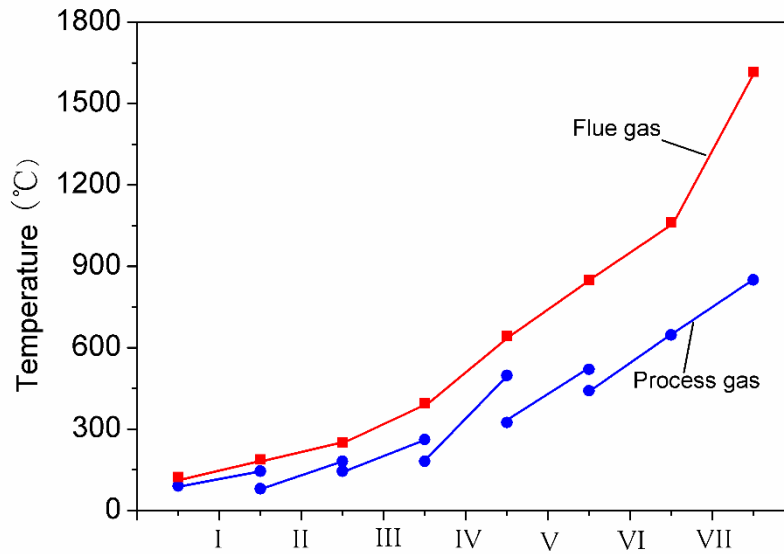


Fig. 6. Temperature profiles of fluids in different Sub-sections

4.1.4. Location of exergy destruction and losses through conventional exergy analysis

Fig. 7(a) was obtained through normalization of value in $y_i(\%)$ column of Table 5. It can be seen from Fig. 7(a) that Sub-section VIII contributes the largest proportion (55.06%) of the total exergy destruction due to the combustion reaction. The second-largest proportion (19.53%) occurs in Sub-section VII where the radiative heat transfer is dominant and the cracking reaction occurs inside the tube reactor. Sub-section VI (HTC) in the convection section also contributes 6.03% of the total exergy destruction followed by the quench system (4.77%). The ECO-I (0.30%), FPH-I (1.21%), ECO-II (1.13%), FPH-II (3.4%), HPSSH (I, II) (2.68%) sub-sections in the convection section have much lower contributions.

Fig. 7(b) shows the distribution of exergy destruction within three sections of the steam cracking furnace. As shown in Fig. 7(b), compared with the radiation section

(74.59%), the quench system and the components in the convection section contribute much less exergy destruction. Thus, the efficient utilization of large amount of exergy should be further investigated for the high exergy efficiency in the radiation section. In the actual process, some heat is lost due to the inadequate insulation measures. In addition, the heat in the flue gas released to the environment is also lost. These heat losses lead to exergy destruction accounting for 5.89% of the total exergy destruction, as shown in Fig. 7.

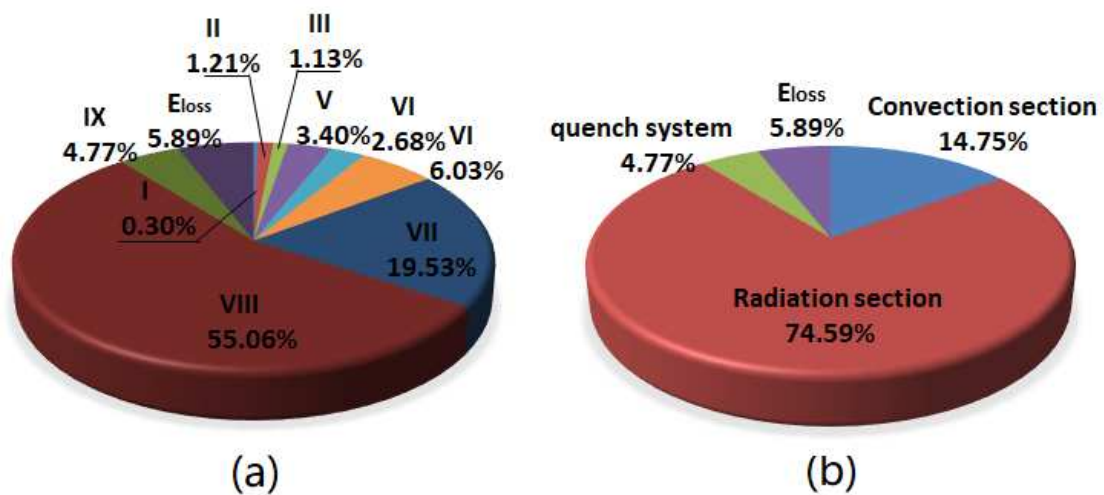


Fig. 7. Distribution of exergy destruction of the steam cracking furnace (a) Distribution of exergy destruction for each component; (b) Distribution of exergy destruction for the convection section, the radiation section and the quench system

4.1.5. Sensitivity analysis

In order to investigate the characteristics of the exergy destruction, it is vital to perform a sensitivity study with each operation parameter varying while all the other values fixed. Fig. 8(a) was obtained when HC mass flow rate changes from 11,000 to 15,000 kg/h while DS mass flow rate is fixed at 4,620 kg/h and COT is fixed at 850 °C.

As shown in Fig. 8(a), the exergy efficiency increases with the increase in HC mass flow rate. This can be explained by that higher HC mass flow rate will promote the occurrence of chemical reactions and consume heat more efficiently.

Fig. 8(b) was obtained when DS mass flow rate changes from 3,600 to 5,440 kg/h while HC mass flow rate is fixed at 13,200 kg/h and COT is fixed at 850°C. As shown in Fig. 8(b), the exergy efficiency decreases with the increase in DS mass flow rate. This can be explained by that higher steam mass flow rate will prevent the occurrence of the side reactions and reduce the residence time, more heat is used to heat the process gas itself not for the cracking reaction. Thus, the heat is consumed less inefficiently.

Fig. 8 (c) was obtained when COT changes from 830 to 870°C while HC mass flow rate is fixed at 13,200 kg/h and DS mass flow rate is fixed at 4,620 kg/h. COT is one of the most important parameter which is controlled for the desired cracking severity. As shown in Fig. 8(c), the exergy efficiency increases with the increase in COT. Although more fuel gas is consumed at the condition of a higher COT, a larger output exergy of the products is obtained. Thus, the exergy efficiency of the whole furnace increases.

In summary, the exergy efficiency has a slight change with the variation in the mass flow rates of HC and DS, and COT. In addition, the changes of the mass flow rates of HC and DS, and COT for a high exergy efficiency may have a negative effect on the production efficiency. For example, with the increase in COT during a period of production, the coke formation rate on the inner surface of the tubular reactor will increase which will decrease the heat transfer efficiency on the inner surface of tubular reactor and also reduced the run length. As a result, the exergy destruction rate of the

steam cracking furnace will be increased during a period of production. Therefore, much attention should be paid to optimize the component structure or reconstruct the overall system in order to improve the thermodynamic efficiency of the steam cracking furnace.

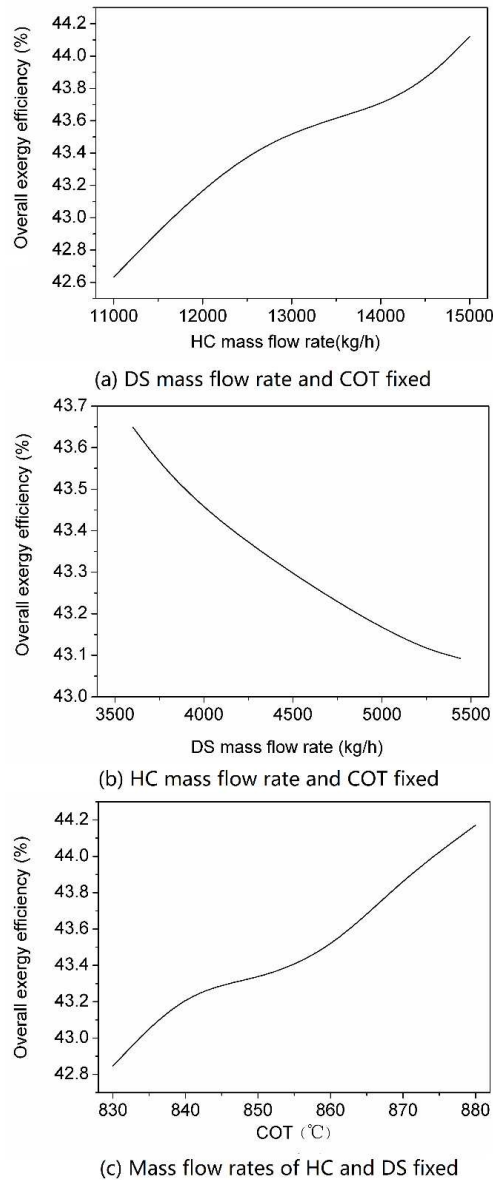


Fig. 8. Effect of the mass flow rates of HC and DS, and COT on the real exergy efficiencies

4.2. Advanced exergy analysis

Through advanced exergy analysis, all parts of exergy destruction within each

component of the steam cracking furnace were evaluated. The results of the advanced exergy analysis are given in Table 6.

Table 6. Results of advanced exergy analysis of the steam cracking furnace

| | $\dot{E}_{D,i}^{EN}$ (kW) | $\dot{E}_{D,i}^{EX}$ (kW) | $\dot{E}_{D,i}^{UN}$ (kW) | $\dot{E}_{D,i}^{AV}$ (kW) | $\dot{E}_{D,i}^{EN,UN}$ (kW) | $\dot{E}_{D,i}^{EN,AV}$ (kW) | $\dot{E}_{D,i}^{EX,UN}$ (kW) | $\dot{E}_{D,i}^{EX,AV}$ (kW) |
|--------------------|------------------------------|------------------------------|------------------------------|------------------------------|---------------------------------|---------------------------------|---------------------------------|---------------------------------|
| Convection section | | | | | | | | |
| I | 21.62 | 24.92 | 7.37 | 39.17 | 6.06 | 15.56 | 1.31 | 23.60 |
| II | 149.56 | 40.63 | 64.73 | 125.46 | 54.53 | 95.03 | 10.20 | 30.43 |
| III | 149.05 | 28.46 | 16.36 | 161.15 | 13.49 | 135.56 | 2.87 | 25.59 |
| IV | 410.70 | 121.54 | 79.86 | 452.38 | 68.10 | 342.59 | 11.76 | 109.79 |
| V | 321.45 | 98.06 | 81.46 | 338.05 | 73.24 | 248.20 | 8.22 | 89.84 |
| VI | 717.71 | 225.75 | 303.56 | 639.90 | 261.19 | 456.51 | 42.36 | 183.39 |
| Radiation section | | | | | | | | |
| VII | 2257.58 | 799.97 | 1407.58 | 1649.97 | 1194.22 | 1063.36 | 213.37 | 586.60 |
| VIII | 8619.83 | 0.00 | 7631.01 | 988.82 | 7631.01 | 988.82 | 0.00 | 0.00 |
| Quench system | | | | | | | | |
| IX | 429.46 | 317.51 | 507.85 | 239.12 | 419.06 | 10.40 | 88.79 | 228.72 |

4.2.1. Unavoidable and avoidable exergy destruction

Fig. 9 indicates the breakdown of unavoidable and avoidable exergy destruction for each component. This figure was presented based on the 3rd and the 4th columns in Table 6. From Fig. 9(a), a significant part (1756.10 kW, 76.04%) of the exergy destruction within the convection section is avoidable. It can be found in Fig. 9(a) that the avoidable exergy destruction within Sub-sections I, III and V increases from top to bottom. The same goes for Sub-sections II, IV and VI. This is because the temperature differences of the sub-sections where the same stream flows through increase from top

to bottom in the convection section. According to the definition of the avoidable exergy destruction, the exergy destruction caused by the temperature difference in the heat exchanger is avoidable. Thus, the avoidable exergy destruction of the sub-sections where the same stream flows through increases from top to bottom in the convection section.

Fig. 9(b) shows the breakdown of unavoidable and avoidable exergy destruction within Sub-section VII (i.e. tube reactor) in the radiation section. As shown in Fig. 9(b), about 53.96% (1649.97 kW) of the exergy destruction within the component is avoidable. This is because the temperature difference of the flue gas and process gas in the component is very large. Therefore, Sub-section VII has great potential to reduce exergy destruction through reducing the temperature difference. However, the unavoidable exergy destruction (1407.58 kW) cannot be ignored. This is because a high-temperature flue gas is necessary for the cracking reaction. Thus, the heat transfer by form of radiation leads to an intensive energy transfer, which causes a large unavoidable exergy destruction.

As shown in Fig. 9(c), most of the exergy destruction (7631.01kW, 88.53%) within Sub-section VIII (i.e. Burner) is unavoidable. This is because most of the exergy destruction is caused by the combustion reactions, only a small part of the exergy destruction is caused by the operating conditions such as the air inlet temperature and the oxygen excess ratio. However, the exergy destruction of 988.82 kW still indicates the energy saving potential of Sub-section VIII cannot be ignored.

Fig. 9(d) shows the breakdown of unavoidable and avoidable exergy destruction

within the quench system, the unavoidable exergy destruction (507.85kW) is larger than the avoidable part (239.12 kW). The avoidable exergy destruction is mainly caused by a large temperature difference between the cracked gas and the steam. Moreover, the cracked gas is cooled rapidly leading to an intensive heat transfer. Therefore, the quench system can reduce the exergy destruction through reducing the temperature difference or using a more effective refrigerants to replace the water.

In summary, Sub-section VII in the radiation section contributes the largest part (35.60%) of the total avoidable exergy destruction of the whole steam cracking furnace, followed by Sub-section VIII (21.34%) in the radiation section and Sub-section VI (13.81%) in the convection section. Therefore, there is the highest energy saving potential in Sub-section VII, followed by Sub-section VIII and Sub-section VI.

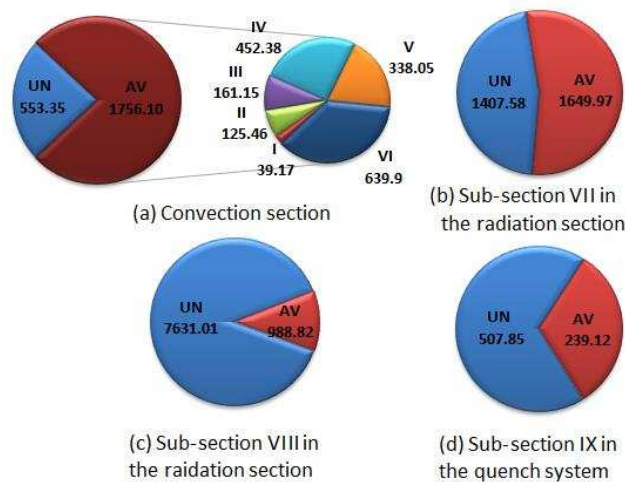


Fig. 9. Advanced exergy analysis into avoidable and unavoidable parts

4.2.2. Endogenous and exogenous exergy destruction

Splitting exergy destruction of each component into endogenous and exogenous parts, $\dot{E}_{D,i}^{EN}$ and $\dot{E}_{D,i}^{EX}$, provides information about how much exergy destruction is

caused by its own structure or operation conditions and how much is by the interacting components. Fig. 10 was presented based on the first and second columns in Table 6. As shown in Fig. 10 (a), about 1770.09 kW (76.65%) of the exergy destruction is endogenous larger than the exogenous part for the convection section. It can also be found that the exogenous exergy destruction in the sub-sections where the same stream flows through increases from top to bottom (i.e. Sub-sections I, III and V, and Sub-sections II, IV and VI). This is because the hydrocarbon feedstock and water/steam streams flow from top to bottom, the exergy destruction of this component is easily affected by the components above. Thus, more exergy destruction is exogenous at the bottom.

Fig. 10 (b) shows the breakdown of endogenous and exogenous exergy destruction within Sub-section VII in the radiation section. A large part (2257.58 kW, 73.84%) of the exergy destruction is endogenous. This is because the exergy destruction in Sub-section VII is mainly caused by the process itself where the high temperature difference and the intensive heat transfer are necessary for providing heat for the cracking reaction inside the tube reactor.

From Fig. 10 (c), all of the exergy destruction in Sub-section VIII (i.e. burner) is endogenous. This is because the combustion process is independent of any other components in the steam cracking furnace. Its input variables such as the mass flow rate of fuel gas and air inlet temperature are not affected by other components. Thus the exergy destruction within the burner is only caused by the combustion process itself.

Fig. 10 (d) indicates the breakdown of endogenous and exogenous exergy

destruction within the quench system. As shown in Fig. 10 (d), the endogenous exergy destruction (429.46 kW) is a little larger than the exogenous part (317.51 kW). This can be explained by two reasons. The reason for endogenous exergy destruction is that the large temperature difference and the intensive heat transfer are necessary to cool the cracked gas rapidly. The reason for the exogenous exergy destruction is that the inlet streams of the quench system are all from the convection and the radiation sections, thus the exergy destruction of this component is easily affected by the other two sections.

In summary, the exergy destruction within the radiation and convection section is mainly caused by the component itself while the exergy destruction within the quench system is caused both by the other components and the component itself.

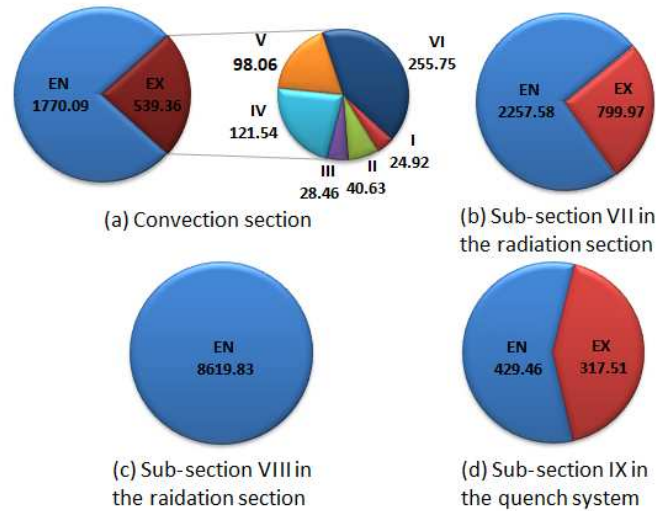


Fig. 10. Advanced exergy analysis into endogenous and exogenous parts

4.2.3. Combination of the splitting

Splitting the avoidable exergy destruction into the endogenous and exogenous parts, $\dot{E}_{D,i}^{AV,EN}$ and $\dot{E}_{D,i}^{AV,EX}$, can guide the improvement direction for each component. Fig. 11 was presented based on the 5th to 8th columns in Table 6. It can be seen from Fig. 11(a),

a large part (1293.46 kW, 73.66%) of avoidable exergy destruction within the convection section is endogenous. Moreover, the exogenous part of the avoidable exergy destruction within the sub-sections where the same stream flows through also increases from top to bottom. In general, the convection section should reduce the exergy destruction by improving the thermodynamic efficiency of the component itself, especially for the components with a larger temperature difference at the bottom of the convection section.

Fig. 11(b) shows the breakdown of endogenous and exogenous parts of the avoidable exergy destruction within Sub-section VII in the radiation section. As shown in Fig. 11(b), the endogenous part (1063.36kW) of the avoidable exergy destruction is larger than the exogenous part (586.60 kW). The reason has been clearly explained in Section 4.2.2. Thus, more improvement measures should focus on Sub-section VII to reduce the exergy destruction.

From Fig. 11(c), all of the avoidable exergy destruction is endogenous. This is because the combustion process in Sub-section VIII is independent of any other components in the steam cracking furnace. Thus the thermodynamic efficiency of Sub-section VIII should be increased through reducing the exergy destruction of the component itself.

Fig. 11(d) shows the breakdown of endogenous and exogenous parts of the avoidable exergy destruction within the quench system. The quench system has an avoidable-exogenous exergy destruction of about 288.72kW, much larger than the avoidable-endogenous exergy destruction of 10.40 kW. Thus, the improvement of the

exergy efficiency of the quench system should consider the reduction of exergy destruction of other components.

In summary, the exergy efficiency of the convection section should be improved through reducing the exergy destruction of each component itself. The exergy efficiency of the radiation section also should be improved by reducing their own exergy destruction. The exergy efficiency of the quench system should be improved mainly through reducing the exergy destruction of the other interacting components.

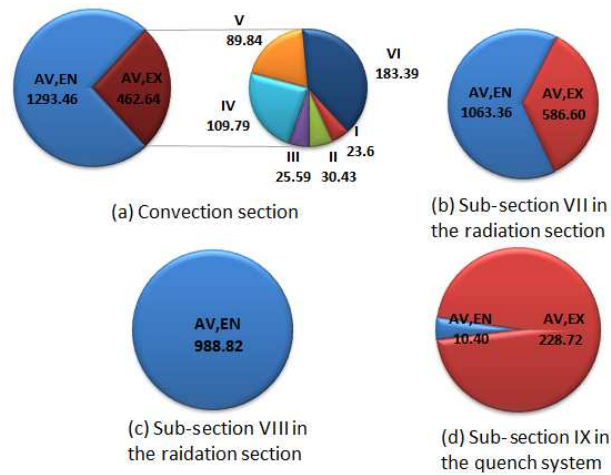


Fig. 11. Advanced exergy analysis into avoidable endogenous and avoidable exogenous parts

5. Conclusion

The conventional and advanced exergy analysis of the steam cracking furnace based on newly developed simulation was performed in this paper, allowing a consistent and detailed evaluation of its energy consumption from the thermodynamic point of view. The conventional exergy analysis evaluates the exergy destruction within each component of the whole furnace. The advanced exergy analysis reveals the real potential for reducing the exergy destruction of each component and points to the new

direction for energy saving. Here, the main conclusions or insights for energy saving significance are list as follows: (1) From the conventional exergy analysis, the combustion process in the radiation section contributes the largest part of the total exergy destruction, followed by the tube reactor in the radiation section and the feed-steam mixture superheater in the convection section. (2) From the advanced exergy analysis, the tube reactor has the highest avoidable exergy destruction, followed by the combustion process and the feed-steam mixture superheater. Therefore, there is high energy saving potential in the three components. (3) The exergy destruction of the convection and radiation sections are mainly caused by the component itself while the exergy destruction of the quench system is caused both by the other components and the component itself. (4) The improvement approaches differ from component to component based on advanced exergy analysis. For example, efforts on improving the convection and radiation sections should be dedicated to themselves while improving the quench system should focus much on other components.

Acknowledgements

This work was supported by National Natural Science Foundation of China (Key Program: 61333010), National Science Fund for Distinguished Young Scholars (61725301), International (Regional) Cooperation and Exchange Project (61720106008) and the Programme of Introducing Talents of Discipline to Universities (the 111 Project) under Grant B17017.

Nomenclature

| | |
|--|---|
| C_H | correlation coefficient, - |
| d | inner diameter, m |
| D | external diameter, m |
| \dot{E} | exergy, kW |
| \dot{E}^{ch} | chemical exergy, kW |
| \dot{E}^{TP} | physical exergy at process state (T, P) , kW |
| $\dot{E}_{BFW,in}$ | inlet exergy of boiler feed water, kW |
| $\dot{E}_{Cracked\ gas}$ | exergy of the cracked gas, kW |
| $\dot{E}_{Cold,in}/\dot{E}_{Cold,out}$ | inlet /outlet exergy of the cold fluid inside the tube, kW |
| $\dot{E}_{Desired\ output}$ | the exergy desired output of the system, kW |
| $\dot{E}_{D,i}$ | exergy destruction of component i , kW |
| $\dot{E}_{D,total}$ | total exergy destruction, kW |
| $\dot{E}_{DS,in}$ | inlet exergy of dilute steam, kW |
| $\dot{E}_{D,i}^{AV}$ | avoidable exergy destruction of component i , kW |
| $\dot{E}_{D,i}^{UN}$ | unavoidable exergy destruction of component i , kW |
| $\dot{E}_{D,i}^{EN}$ | endogenous exergy destruction of component i , kW |
| $\dot{E}_{D,i}^{EX}$ | exogenous exergy destruction of component i , kW |
| $\dot{E}_{D,i}^{AV,EN}$ | avoidable endogenous exergy destruction of component i , kW |
| $\dot{E}_{D,i}^{AV,EX}$ | avoidable exogenous exergy destruction of component i , kW |
| $\dot{E}_{D,i}^{UN,EN}$ | unavoidable endogenous exergy destruction of component i , kW |
| $\dot{E}_{D,i}^{UN,EX}$ | unavoidable exogenous exergy destruction of component i , kW |

| | |
|--------------------------------------|--|
| $\dot{E}_{F,i}$ | exergy of feedstock in component i , kW |
| $\dot{E}_{Feed,in}$ | inlet exergy of the feedstock, kW |
| \dot{E}_{Fuel} | inlet exergy of the fuel gas, kW |
| $\dot{E}_{Flue\ gas}$ | outlet exergy of the flue gas, kW |
| $\dot{E}_{Hot,in}/\dot{E}_{Hot,out}$ | inlet /outlet exergy of the hot fluid outside the tube, kW |
| $\dot{E}_{HC,in}$ | inlet exergy of hydrocarbon feedstock, kW |
| \dot{E}_{Hp} | inlet exergy of the high pressure steam, kW |
| \dot{E}_{in} | total input exergy of the system, kW |
| $\dot{E}_{L,i}$ | exergy loss of component i , kW |
| $\dot{E}_{Product}$ | product exergy, kW |
| $\dot{E}_{p,i}^{EN}$ | product exergy of component i in the theoretical condition, kW |
| $\dot{E}_{p,i}$ | product exergy of component i , kW |
| $\dot{E}_{p,i}^R$ | product exergy of component i in the real condition, kW |
| $\dot{E}_{P,out}$ | product exergy of the system, kW |
| \dot{E}_{Used} | used exergy of the system, kW |
| f | Fanning friction factor, - |
| F | radiative view factor, - |
| ΔG_f^0 | standard Gibbs energy of formation, J/mol |
| h_c | convective heat-transfer coefficient of the process gas, W/m ² /K |
| h_f | convective heat-transfer coefficient of the flue gas, W/m ² /K |
| H | enthalpy, kJ/kg |
| \dot{I}_i | internal exergy destruction of component i , kW |
| N | total exchange factor, - |
| S | entropy, kJ/kg/K |

| | |
|------------------|--|
| P | pressure of process stream, Pa |
| P_0 | initial pressure of the process stream, Pa |
| P_{in} | inlet pressure of the process stream in a tube segment, Pa |
| P_{out} | outlet pressure of the process stream in a tube segment, Pa |
| ΔP | pressure drop of each component, Pa |
| q | heat flux of the internal surface of the tube, $\text{kJ/m}^2\text{s}$ |
| q_{flux} | heat flux of the external surface of the tube, $\text{kJ/m}^2\text{s}$ |
| q_{inci} | incident radiative heat flux, $\text{kJ/m}^2\text{s}$ |
| Q_{ab} | heat absorbed by all reactor coils, kW |
| Q_{flue} | enthalpy change between the inlet fuel and air entering the furnace and the hot flue gas leaving the furnace, kW |
| Q_{flue}^{con} | convective heat from the flue gas to tubes, kW |
| Q_{flue}^{rad} | radiative heat from the flue gas to tubes, kW |
| Q_{wall}^{rad} | radiative heat to from the furnace wall to tubes, kW |
| Q_{loss} | heat loss of the steam cracking furnace, kW |
| Q_r | heat released by fuel combustion, kW |
| R | gas constant, $8.31451 \text{ kJ/kmol/K}$ |
| r_b | bend radius, m/s |
| T | temperature of process stream, K |
| T_{flue} | flue gas bridge wall temperature, K |
| T_0 | initial temperature of the process stream, K |
| T_w | external skin temperature of the tube, K |
| ΔT_{min} | pin point temperature, K |
| n | molar flow, mol/s |
| u | velocity, m/s |
| X_i^0 | molar standard chemical exergy, kJ |
| y_i | mole fraction of the components, - |
| $y_{D,k}$ | exergy loss ratio, - |

Z global composition of material stream, -

Greek symbols

σ Stefan–Boltzmann constant, $\text{W/m}^2/\text{K}^4$, $\sigma = 5.672 \times 10^{-8}$

β ratio of radiative heat flux to convective heat flux

λ thermal conductivity of the flue gas, W/m/K

λ_w metal thermal conductivity, W/m/K

ρ density, kg/m^3

ε_{con} conventional exergy efficiency, -

ε_g blackness of the flue gas, -

ε_t blackness of the tube wall, -

ε_{rat} rational exergy efficiency, -

ε_i exergy efficiency of component i , -

ε_w blackness of the furnace wall, -

$\varepsilon_{whole\ furnace}$ rational exergy efficiency of the whole furnace, -

ψ correlation coefficient of the tube bundle, -

ξ local drag coefficient, -

Subscript

D destruction

L loss

min minimum

P product

Acronyms

AV avoidable

CIT coil inlet temperature

COT coil outlet temperature

DS dilute steam

| | |
|-------|---------------------------------|
| ECO | economizer |
| EN | endogenous |
| EX | exogenous |
| FPH | feed preheater |
| HC | hydrocarbon feedstock |
| HP | high pressure steam |
| HPSSH | high pressure steam superheater |
| HTC | feed-steam mixture superheater |
| TLE | transfer line exchanger |
| IRHF | incident radiative heat flux |
| UN | unavoidable |

References

- [1] Chen Y, Han Y, Zhu Q. Energy and environmental efficiency evaluation based on a novel data envelopment analysis: An application in petrochemical industries. *Appl. Therm. Eng.* 2017;119:156-64.
- [2] Ren T, Patel M, Blok K. Olefins from conventional and heavy feedstocks: Energy use in steam cracking and alternative processes. *Energy*. 2006;31:425-51.
- [3] J.J. Liu, Y. Guo, L.J. Zhang. Process simulation of the convection section of cracking furnace based on Asepen Plus user model. *Tianjin Chem. Ind.* 2009;23:25-9.
- [4] Y. Zhou, D.Z. Yang. Simulation and optimum design for convection section of ethylene cracking furnace. *Chem. Eng. (China)*. 2010;38.
- [5] Plus A. Ten Canal Park, Cambridge (MA) 02141. Aspen Technology Inc.2009.
- [6] Ibrahim HA-H, Al-Qassimi M. Simulation of heat transfer in the convection section of fired process heaters. *Period .Polytech. Chem. Eng.* 2010;54:33.
- [7] De Schepper SCK, Heynderickx GJ, Marin GB. Modeling the evaporation of a hydrocarbon feedstock in the convection section of a steam cracker. *Comput. Chem. Eng.* 2009;33:122-32.
- [8] De Schepper SCK, Heynderickx GJ, Marin GB. Coupled simulation of the flue gas and process gas side of a steam cracker convection section. *AIChE J.* 2009;55:2773-87.
- [9] Hu G, Yuan B, Zhang L, Li J, Du W, Qian F. Coupled simulation of convection section with dual stage steam feed mixing of an industrial ethylene cracking furnace. *Chem. Eng. J.* 2016;286:436-46.
- [10] Heynderickx GJ, Oprins AJM, Marin GB, Dick E. Three-dimensional flow patterns in cracking furnaces with long-flame burners. *AIChE J.* 2001;47:388-400.
- [11] Oprins AJM, Heynderickx GJ, Marin GB. Three-dimensional asymmetric flow and temperature fields in cracking furnaces. *Ind. Eng. Chem. Res.* 2001;40:5087-94.
- [12] Oprins AJM, Heynderickx GJ. Calculation of three-dimensional flow and pressure fields in cracking furnaces. *Chem. Eng. Sci.* 2003;58:4883-93.
- [13] Stefanidis GD, Heynderickx GJ, Marin GB. Development of reduced combustion mechanisms for premixed flame modeling in steam cracking furnaces with emphasis on NO emission. *Energy & Fuels*. 2006;20:103-13.
- [14] Lan X, Gao J, Xu C, Zhang H. Numerical Simulation of Transfer and Reaction Processes in Ethylene Furnaces. *Chem. Eng. Res. Des.* 2007;85:1565-79.
- [15] Han YL, Xiao R, Zhang MY. Combustion and Pyrolysis Reactions in a Naphtha Cracking Furnace. *Chem. Eng. Technol.* 2010;30:112-20.
- [16] Habibi A, Merci B, Heynderickx GJ. Impact of radiation models in CFD simulations of steam cracking furnaces. *Comput. Chem. Eng.* 2007;31:1389-406.
- [17] Hu G, Schietekat CM, Zhang Y, Qian F, Heynderickx G, Van Geem KM, et al. Impact of radiation models in coupled simulations of steam cracking furnaces and reactors. *Ind. Eng. Chem. Res.* 2015;54:2453-65.
- [18] Zhang Y, Reyniers PA, Du W, Qian F, Van Geem KM, Marin GB. Incident Radiative Heat Flux Based Method for the Coupled Run Length Simulation of Steam Cracking Furnaces. *Ind. Eng. Chem. Res.* 2017;56:4156-72.
- [19] Tuomaala M, Hurme M, Leino A-M. Evaluating the efficiency of integrated systems in the process industry—Case: Steam cracker. *Appl. Therm. Eng.* 2010;30:45-52.
- [20] Saidur R, Ahamed JU, Masjuki HH. Energy, exergy and economic analysis of industrial boilers.

Energy Policy. 2010;38:2188-97.

[21] Alghany SANAA, Morsy BK, Abd El-Rahman AA, Ieee. A Study of Exergy Analysis for Combustion in Direct Fired Heater (Part I). 2014 International Conference on Mathematics and Computers in Sciences and in Industry2014. p. 139-48.

[22] Shekarchian M, Zarifi F, Moghavvemi M, Motasemi F, Mahlia T. Energy, exergy, environmental and economic analysis of industrial fired heaters based on heat recovery and preheating techniques. *Energ. Convers. Manage.* 2013;71:51-61.

[23] Alizadeh M, Sadrameli SM. Modeling of Thermal Cracking Furnaces Via Exergy Analysis Using Hybrid Artificial Neural Network–Genetic Algorithm. *J. Heat Transf.-Trans. ASME.* 2016;138:1-11.

[24] Yang Q, Qian Y, Kraslawski A, Zhou H, Yang S. Advanced exergy analysis of an oil shale retorting process. *Applied Energy.* 2016;165:405-15.

[25] Chen J, Havtun H, Palm B. Conventional and advanced exergy analysis of an ejector refrigeration system. *Applied Energy.* 2015;144:139-51.

[26] Tsatsaronis G, Morosuk T. Advanced exergetic analysis of a novel system for generating electricity and vaporizing liquefied natural gas. *Energy.* 2010;35:820-9.

[27] Gholamian E, Hanafizadeh P, Ahmadi P. Advanced exergy analysis of a carbon dioxide ammonia cascade refrigeration system. *Appl. Therm. Eng.* 2018;137:689-99.

[28] Gong S, Goni Boulama K. Parametric study of an absorption refrigeration machine using advanced exergy analysis. *Energy.* 2014;76:453-67.

[29] Olaleye AK, Wang M, Kelsall G. Steady state simulation and exergy analysis of supercritical coal-fired power plant with CO₂ capture. *Fuel.* 2015;151:57-72.

[30] Zimmermann H. Ethylene WR. Ullmann's Encyclopedia of Industrial Chemistry. Weinheim, Germany: Wiley-VCH Verlag GmbH & Co, KGaA2000.

[31] Karimzadeh R, Godini HR, Ghashghaee M. Flowsheeting of steam cracking furnaces. *Chem. Eng. Res. Des.* 2009;87:36-46.

[32] McAdams WH. Heat transmission, 2nd ed: McGraw-Hill, New York; 1958.

[33] Colburn AP. A method of correlating forced convection heat-transfer data and a comparison with fluid friction. *Int J Heat Mass Tran.* 1964;7:1359-84.

[34] Mandhani VK, Chhabra RP, Eswaran V. Forced convection heat transfer in tube banks in cross flow. *Chem Eng Sci.* 2002;57:379-91.

[35] Khan WA, Culham JR, Yovanovich MM. Convection heat transfer from tube banks in crossflow: Analytical approach. *Int. J. Heat Mass Tran.* 2006;49:4831-8.

[36] Bergman TL, Incropera FP. Fundamentals of heat and mass transfer: John Wiley & Sons; 2011.

[37] Van Geem KM, Hudebine D, Reyniers MF, Wahl F, Verstraete JJ, Marin GB. Molecular reconstruction of naphtha steam cracking feedstocks based on commercial indices. *Comput. Chem. Eng.* 2007;31:1020-34.

[38] Van Geem KM, Žajdlík R, Reyniers M-F, Marin GB. Dimensional analysis for scaling up and down steam cracking coils. *Chem. Eng. J.* 2007;134:3-10.

[39] Liu Z, Winterton RHS. A general correlation for saturated and subcooled flow boiling in tubes and annuli, based on a nucleate pool boiling equation. *Int. J. Heat Mass Tran.* 1991;34:2759-66.

[40] Gungor KE, Winterton RHS. A general correlation for flow boiling in tubes and annuli. *Int. J. Heat Mass Tran.* 1986;29:351-8.

[41] Szargut J, Morris D, Steward F. Exergy Analysis of Thermal, Chemical, and Metallurgical Processes.

Hemisphere, New York, 1988.

[42] Ghannadzadeh A, Thery-Hetreux R, Baudouin O, Baudet P, Floquet P, Joulia X. General methodology for exergy balance in ProSimPlus® process simulator. *Energy*. 2012;44:38-59.

[43] Kotas TJ. *The exergy method of thermal plant analysis*: Butterworth-Heinemann; 1985. p. 288-92.

[44] Yang Y, Wang L, Dong C, Xu G, Morosuk T, Tsatsaronis G. Comprehensive exergy-based evaluation and parametric study of a coal-fired ultra-supercritical power plant. *Applied Energy*. 2013;112:1087-99.

[45] Cziesla F, Tsatsaronis G, Gao Z. Avoidable thermodynamic inefficiencies and costs in an externally fired combined cycle power plant. *Energy*. 2006;31:1472-89.

[46] Phil M, Kelly S, der Fakultät V. *Energy Systems Improvement based on Endogenous and Exogenous Exergy Destruction*. PhD thesis. : Technische University Berlin, Germany; 2008.

[47] Morosuk T, Tsatsaronis G. Advanced exergy analysis for chemically reacting systems—application to a simple open gas-turbine system. *Int. J. Thermodynamics*. 2009;12:105-11.

[48] Boyano A, Blanco-Marigorta A-M, Morosuk T, Tsatsaronis G. Steam Methane Reforming System for Hydrogen Production: Advanced Exergetic Analysis. *Int. J. Thermodynamics*. 2012.